Molecular and Electronic Structure of the Confacial Diosmium(III) Nonabromide Complex Anion. X-ray Crystallography of $Rb_3Os_2Br_9$ and Direct Comparisons of $[Os_2Br_9]^{3-}$ with $[Ru_2Br_9]^{3-}$

Stephen F. Gheller, Graham A. Heath,* David C. R. Hockless, David G. Humphrey, and John E. McGrady

Research School of Chemistry, The Australian National University, Canberra, ACT 0200, Australia

Received August 10, 1993®

The single-crystal X-ray structure of $Rb_3Os_2Br_9$ provides the first crystallographic definition of a diosmium confacial nonahalide. $Rb_3Os_2Br_9$ crystallizes in the hexagonal space group $P6_3/m$ [a/Å = 7.401(1), c/Å = 18.098(4)], Z = 2, conferring strict D_{3h} symmetry on the complex anion. The internal geometry of the 10-e ($5d^5/5d^5$) binuclear complex [β = 66.54(5)°; Os–Os = 2.779(1), Os–Br_t = 2.499(1), Os–Br_{br} = 2.532(2) Å] is consistent with significant net σ bonding [$\sigma^2\delta_\pi{}^4\delta_\pi{}^{*4}$]. Comparative SCF–X$\alpha$–SW calculations on $[Os_2Br_9]^{3-}$ and $[Ru_2Br_9]^{3-}$ reinforce the picture of greater metal–metal interaction in the heavier (third-row) species. The optical spectra of $[Os_2Br_9]^{3-}$ and $[Ru_2Br_9]^{3-}$ bear a qualitative resemblance; the main features are attributed to superposition of metal-based $\sigma \rightarrow \sigma^*$ ($6a_1' \rightarrow 5a_2''$) and ligand-field ($6a_1' \rightarrow 9e'$) transitions in the visible/near-UV envelope and, at higher energy, to intense $Br_{br/t}$-to-M_2 charge transfer to π_δ^* and π_δ ($7e''$, $9e'$) arising from the single-ion e_g levels. The $\sigma \rightarrow \sigma^*$ band is located near 24 000 cm^{-1} in $[Os_2Br_9]^{3-}$ and near 20 000 cm^{-1} in $[Ru_2Br_9]^{3-}$. An electron-exchange term (K) of the order 8000 cm^{-1} is implied in both cases.

Introduction

We recently reported the discovery and electrochemical characterization of long-sought $[Os_2(\mu\text{-}Br)_3Br_6]^{3-}$ and its chloro analogue,[1,2] via reductive halide extrusion from edge-sharing[3] $[Os^{IV}_2(\mu\text{-}X)_2X_8]^{2-}$ (X = Br, Cl) at −30 °C. This contrasts with the spontaneous formation of triply-bridged $[Ru_2(\mu\text{-}Br)_3Br_6]^{3-}$, which tends to dominate Ru^{III}/Br chemistry.[4,5] The confacial nonahalides are of particular interest in tervalent osmium chemistry because of their structural and electronic relationship to $[OsX_6]^{3-}$ and to newly characterized[1] $[Os^{III}_2(\mu\text{-}X)_2X_8]^{4-}$, as well as to directly bonded $[Os^{III}_2X_8]^{2-}$ (X = Br, Cl).[6] After extensive efforts to define the elusive $[Os_2X_9]^{z-}$ system crystallographically, in either the III,III or IV,IV oxidation state,[1] we now report a precise single-crystal X-ray study of $Rb_3Os_2Br_9$. The new structural data enable systematic comparisons of the physical properties of $[Os_2Br_9]^{3-}$ and $[Ru_2Br_9]^{3-}$. These 10 d-electron (10-e) systems are of particular significance, both for measurement and computation, because their net metal–metal interaction is purely σ in character. The SCF–Xα–SW calculations summarized below provide a firm basis for assigning the optical spectra of $[Os_2Br_9]^{3-}$ and $[Ru_2Br_9]^{3-}$, and a consistent picture emerges of quantifiably greater metal–metal interaction in the third-row (5d) species.

Experimental Methods

A purple hexagonal plate of $Rb_3Os_2Br_9$, grown by slow evaporation from an aqueous solution of $[(C_2H_5)_4N]_3Os_2Br_9$ and RbBr (1:3), was mounted on a glass fiber and examined at 23 °C using a rotating-anode Rigaku AFC6R diffractometer in the $\omega/2\theta$ mode (Table 1). Least-squares refinement of setting angles for 25 high-angle reflections in the range 97.31 < 2θ < 99.91° provided accurate unit-cell constants corresponding to a primitive hexagonal cell (Laue class 6/m). Diffraction data ($\pm h,+k,+l$) were collected between 3 and 120° (R_{merge} = 0.13). The data were corrected for Lorentz and polarization effects and also for severe absorption using a face-indexed analytical procedure; calculated transmission factors ranged from 0.03 to 0.38. Decay was <1% overall. No extinction correction was necessary. The space group was unambiguously defined as $P6_3/m$ (No. 176)[7] in accord with systematic absences and statistical analysis of the intensity distribution. The structure was solved by direct methods (SIR 88)[8] and expanded by Fourier techniques (DIRDIF92).[9] The five unique atoms, Os, Br(1), Br(2), Rb(1), and Rb(2), were refined anisotropically. Final atomic coordinates and displacement parameters are listed in Table 2. Neutral-atom scattering factors, and values for $\Delta F'$ and $\Delta F''$, were from standard sources.[10,11] Anomalous dispersion effects were included in F_c.[12] All calculations were performed using the teXsan software package.[13]

Spin-restricted SCF–Xα–SW calculations were performed using the standard codes of Case and Cook.[14] Atomic α values were those of Schwartz,[15] valence-electron weighted averages were used for the intersphere and outer-sphere regions. Overlapping atomic sphere radii were set at 89% of corresponding atomic number raddi, following Norman.[16] A tangential Watson sphere[17] of charge +3 was placed at the outer-sphere radius. Spherical standards up to L = 2, 3, and 5 were used for Br, Os/Ru, and outer regions, respectively, and relativistic radial wave functions were used for Os. Transition energies were calculated using the Slater transition state method,[18] while oscillator strengths were calculated using Noodleman's procedure.[19] Our computational methods closely replicate the benchmark calculation[20] on $[Ru_2Cl_9]^{3-}$.

* Abstract published in *Advance ACS Abstracts*, August 1, 1994.

(1) Heath, G. A.; Humphrey, D. G. *J. Chem. Soc., Chem. Commun.* **1990**, 672.
(2) Humphrey, D. G. Ph.D Thesis, Australian National University, 1992.
(3) (a) Cotton, F. A.; Duraj, S. A.; Hinkley, C. C.; Matusz, M.; Roth, W. J. *Inorg. Chem.* **1984**, *23*, 3080. (b) Bruns, M.; Preetz, W. *Z. Anorg. Allg. Chem.* **1986**, *537*, 88.
(4) Fergusson, J. E.; Greenaway, A. M. *Aust. J. Chem.* **1978**, *31*, 497.
(5) Coombe, V. T.; Heath, G. A.; Stephenson, T. A.; Vattis, D. K. *J. Chem. Soc., Dalton Trans.* **1983**, 2307.
(6) (a) Fanwick, P. E.; Tetrick, S. M.; Walton, R. A. *Inorg. Chem.* **1986**, *25*, 4546. (b) Gheller, S. F.; Heath, G. A.; Raptis, R. G. *J. Am. Chem. Soc.* **1992**, *114*, 7924.
(7) *International Tables for Crystallography*; Hahn, T.; Ed.; Reidel Publishing Co.: Dordrecht, The Netherlands, 1983; Vol. A, Table 176, p 555.
(8) Burla, M. C.; Camalli, M.; Cascavano, G.; Giacovazzo, C.; Polidovi, G.; Spagna, R.; Viterbo, D. *J. Appl. Crystallogr.* **1989**, *22*, 389.
(9) Beurskens, P. T.; Admiraal, G.; Beurskens, G.; Bosman, W. P.; Garcia-Granda, S.; Gould, R. O.; Smits, J. M. M.; Smykalla, C. *The DIRDIF program*; Technical Report of the Crystallography Laboratory; University of Nijmegen: Nijmegen, The Netherlands, 1992.
(10) Cromer, D. T.; Waber, J. T. *International Tables for X-ray Crystallography*; The Kynoch Press: Birmingham, England, 1974; Vol. IV, Table 2.2A.
(11) Creagh, D. C.; McAuley, W. J. *International Tables for X-ray Crystallography*; Wilson, A. J. C., Ed.; Kluwer Academic Publishers: Boston, MA, 1992; Vol. C, Table 4.2.6.8, p 219.
(12) Ibers, J. A.; Hamilton, W. C. *Acta Crystallogr.* **1964**, *17*, 781.
(13) *The teXsan Crystal Structure Analysis Package*; Molecular Structure Corp.: The Woodlands, TX, 1985, 1992.
(14) Cook, M.; Case, D. A. *QCPE* **1982**, *4*, No. 465.
(15) Schwarz, L. *Theor. Chim. Acta.* **1974**, *34*, 225.
(16) Norman, J. G. *Mol. Phys.* **1976**, *31*, 1191.
(17) Watson, R. E. *Phys. Rev.* **1958**, *111*, 1108.

0020-1669/94/1333-3986$04.50/0

Table 1. Crystallographic Data for $Rb_3Os_2Br_9$

empirical formula	$Rb_3Os_2Br_9$
M_r	1355.94
space group	$P6_3/m$ (No. 176)
cryst system	hexagonal
a/Å	7.401(1)
c/Å	18.098(4)
V/Å^3	858.5(3)
D_{calc}/g·cm^{-3}	5.24 (Z = 2)
cryst dimens/mm	0.135 × 0.126 × 0.017
radiation (Cu Kα) wavelength/Å	1.5418
2θ ($\pm h,+k,+l$) (with R_{merge} = 0.13)	3–120°
no. of measd reflcns (23 °C)	997
no. of unique reflcns	454
no. of obsd reflcns $I > 3\sigma(I)$	348
no. of params	25
abs coeff μ/mm^{-1}	62.2
$R = \Sigma(\|F_o\| - \|F_c\|)/\Sigma\|F_o\|$	0.048
$R_w = [\Sigma w(\|F_o\| - \|F_c\|)^2/\Sigma(wF_o^2)]^{1/2}$	0.042

Table 2. Atomic Coordinates and Isotropic Displacement Parameters (Å^2) for $Rb_3Os_2Br_9$[a]

atom	x	y	z	B_{eq}
Os(1)	0.6667	0.3333	0.67324(4)	1.25(1)
Rb(1)	1.0000	1.0000	0.7500	2.65(3)
Rb(2)	0.3333	−0.3333	0.9318(1)	3.05(3)
Br(1)	0.8249(2)	0.6512(2)	0.59328(6)	2.38(3)
Br(2)	0.5018(3)	0.0030(3)	0.7500	1.96(4)

[a] $B_{eq} = {}^8/_3\pi^2\{U_{11}(aa^*)^2 + U_{22}(bb^*)^2 + U_{33}(bb^*)^2 + 2U_{12}aa^*bb^* \times \cos\gamma + 2U_{13}aa^*cc^* \cos\beta + 2U_{23}bb^*cc^* \cos\alpha\}$.

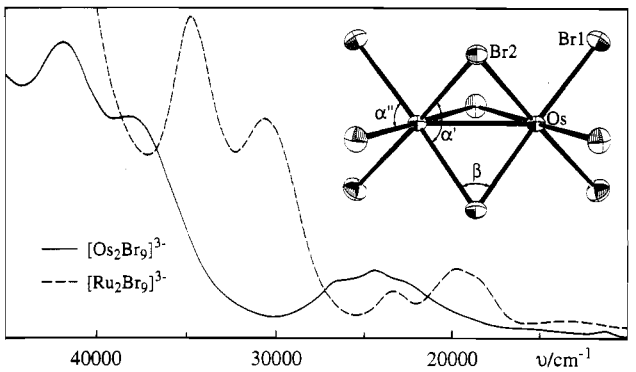

Figure 1. Electronic spectra of $[Os_2Br_9]^{3-}$ (—) and $[Ru_2Br_9]^{3-}$ (- - -) Inset: Thermal ellipsoid plot (50% probability) for $[Os_2Br_9]^{3-}$.

Results and Discussion

Crystal Structure. Purple $Rb_3Os_2Br_9$, derived by metathesis from $(Bu_4N)_3Os_2Br_9$, is characterized by two strong sharp far-IR bands at 219 and 227 cm^{-1} (ν(Os–Br), in polythene). Interestingly, the rubidium salt crystallises in the hexagonal space group $P6_3/m$ (Z = 2), isomorphous with known $A_3M_2X_9$ structures[21] where A = K rather than Cs. The alkali cations, 2 × Rb(1) and 4 × Rb(2), are found in two distinct cavities in the unit cell (each with 12 neighboring bromides) corresponding to positions (a) and (f) in ref 7. A 3-fold rotation axis passes through the two osmium atoms of the confacial bioctahedron, and the bridging bromide ligands lie on the perpendicular mirror plane (Figure 1). The complex anion is thus defined by just three atoms, Os(1), Br(1), and Br(2), as illustrated, and the overall structure is very precisely determined. Table 3 compares pertinent internuclear distances and angles with those determined elsewhere[22] for $[Ru_2Br_9]^{3-}$. The measured internuclear M–M distance (2.78 Å) is shorter by 0.10 Å, and the internal angles of the $OsBr_3Os$ core (α', β) point to significantly stronger metal–metal attraction than in $[Ru_2Br_9]^{3-}$, according to established criteria. The compression factor[23] (unity for an ideal bioctahedron) equals 0.967 for $[Os_2Br_9]^{3-}$; *cf.* 1.001 for $[Ru_2Br_9]^{3-}$. Nonetheless, the terminal $OsBr_3$ moiety approaches ideal octahedral geomery (α'' = 90°), so that the capping ligand array does not contribute to the electronic trigonal-field perturbation imposed on each metal ion.

Table 3. Structural Parameters[a] for $[Os_2Br_9]^{3-}$ and $[Ru_2Br_9]^{3-}$

distances and angles		$[Os_2Br_9]^{3-}$	$[Ru_2Br_9]^{3-}$
M–M	d/Å	2.779(1)	2.880(3)
M–Br_{br}	r_1/Å	2.532(2)	2.512(9)
M–Br_t	r_2/Å	2.499(1)	2.508(9)
M–Br_{br}–M	β/deg	66.54(5)	69.97(9)
Br_{br}–M–Br_{br}	α'/deg	92.78(4)	90.4(1)
Br_t–M–Br_t	α''/deg	89.83(4)	90.3(1)

[a] In the ideal bioctahedron, $r_1 = r_2$, $\alpha' = \alpha'' = 90°$, and $\beta = 70.25°$.

Electronic Structure. Molecular orbital calculations are already available for $[Ru_2Cl_9]^{3-}$.[20] The new structural data (Table 3) provide the first opportunity for a similar analysis of $[Os_2Br_9]^{3-}$ and for direct comparison of $[Os_2Br_9]^{3-}$ with $[Ru_2Br_9]^{3-}$ within the SCF–Xα–SW methodology. The parent monomers $[OsBr_6]^{3-}$ and $[RuBr_6]^{3-}$ were also examined to explore the relationship between MX_6 and M_2X_9 ligand fields and to calibrate the estimation of Br-to-M(III) charge-transfer band energies in the dimers (see below).

In the confacial bioctahedral complexes the frontier-orbital domain is characterized as expected by a manifold of metal-dominated levels with the labels $6a_1'$, 8e', 6e'', $5a_2''$, 7e'', and 9e', which may also be designated as σ, δ_π, δ_π^*, σ^*, π_δ^*, and π_δ (Figure 2). Essentially, σ, δ_π, δ_π^*, and σ^* are derived from the single-ion t_{2g} orbitals, and π_δ^* and π_δ are derived from the single-ion e_g orbitals. These designations are chosen to reflect that, in the ideal confacial bioctahedron, 6e'' and 8e' approach ($^2/_3\delta + {}^1/_3\pi$) bond character, while 7e'' and 9e' approach ($^2/_3\pi + {}^1/_3\delta$).[24] The δ quality of the δ_π and δ_π^* wave functions, and likewise of π_δ and π_δ^*, is reflected in the presence of *two* nodal surfaces (one planar, one curved) which intersect at right angles along the M–M vector.

As "34-electron" systems[5] with a 10 d-electron count, both complexes have a closed-shell ground state with the configuration $[\sigma^2\delta_\pi^4\delta_\pi^{*4}]$ and a formal bond order of unity. Nonetheless, in organosoluble salts of $[Ru_2Br_9]^{3-}$,[5,25] the magnetic data suggested relatively modest metal–metal bonding and the presence of a thermally accessible triplet state. By comparison, $[Os_2Br_9]^{3-}$ has much suppressed magnetic susceptibility (μ_{eff}/μ_B (293 K) per metal ion = 0.25 for Os but = 1.1 for Ru) in accord with the shorter metal–metal distance. The greater voltammetric separation of the 34/33e and 33/32e couples (0.72 V in $[Os_2Br_9]^{3-}$ *vs* 0.51 V in $[Ru_2Br_9]^{3-}$)[1] is also a classical indication[26] of stronger metal–metal interactions in the diosmium species. The quantitative aspects of the Xα calculation clarify these marked differences in physical properties. Most importantly, the computed σ/σ^* separation is 14 900 cm^{-1} in $[Os_2Br_9]^{3-}$, cf. 9400 cm^{-1} in $[Ru_2Br_9]^{3-}$, an increase of 60%. Similarly, the δ_π/δ_π^* splitting which is negligible in $[Ru_2Br_9]^{3-}$ (as in $[Ru_2Cl_9]^{3-}$)[20] reaches

(18) Slater, J. C. *Adv. Quantum Chem.* **1972**, *6*, 1.
(19) Noodleman, L. *J. Chem. Phys.* **1976**, *64*, 2343.
(20) Bursten, B. E.; Cotton, F. A.; Fang, A. *Inorg. Chem.* **1983**, *22*, 2127.
(21) (a) Saillant, R.; Jackson, R. B.; Streib, W. E.; Folting, K.; Wentworth, R. A. D. *Inorg. Chem.* **1971**, *10*, 1453. (b) Fergusson, J. E.; Sherlock, R. R. *Aust. J. Chem.* **1977**, *30*, 1445.
(22) Appleby, D.; Hitchcock, P. B.; Hussey, C. L.; Ryan, T. A.; Sanders, J. R.; Seddon, K. R.; Turp, J. E.; Zora, J. A. *J. Chem. Soc., Dalton Trans.* **1990**, 1879.
(23) Cotton, F. A.; Ucko, D. A. *Inorg. Chim. Acta* **1972**, *6*, 161.
(24) (a) Trogler, W. C. *Inorg. Chem.* **1980**, *19*, 697. (b) Summerville, R. H.; Hoffmann, R. *J. Am. Chem. Soc.* **1979**, *101*, 3821.
(25) Kennedy, B. J.; Heath, G. A.; Khoo, T. J. *Inorg. Chim. Acta* **1991**, *190*, 265.
(26) Brown, D. B.; Wroblenski, J. T. *Mixed Valence Compounds*; Brown, D. B., Ed.; Reidel Publishing Co.: Dordrecht, The Netherlands, 1980; p 49.

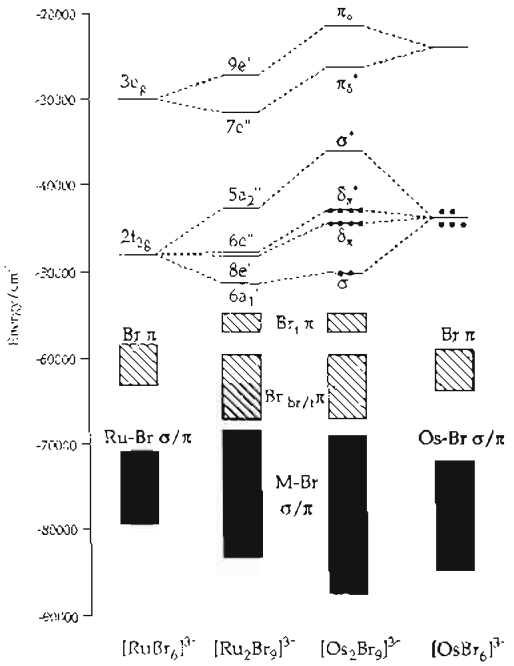

Figure 2. Comparative molecular orbital diagram for $[MBr_6]^{3-}$ and $[M_2Br_9]^{3-}$. The $[Os_2Br_9]^{3-}$ energy level diagram has been placed so that the uppermost Br_t π levels coincide with those of $[Ru_2Br_9]^{3-}$. Similarly, each $[MBr_6]^{3-}$ diagram is uniformly shifted so that the t_{2g} level coincides with the barycenter of the weakly interacting {8e',6e''} manifold of the corresponding $[M_2Br_9]^{3-}$ complex.

1500 cm^{-1} in $[Os_2Br_9]^{3-}$, though of course making no net contribution to bonding.

Optical Spectra. The optical spectra of $[Ru_2Br_9]^{3-}$ and $[Os_2Br_9]^{3-}$ bear a marked family resemblance, as seen in Figure 1. The calculated transition energies and oscillator strengths of the electronic transitions of $[Ru_2Br_9]^{3-}$ and $[Os_2Br_9]^{3-}$ are summarized in Table 4. The tendency of the Xα method to underestimate the energy of XMCT transitions is well documented.[27] A uniform adjustment of the order of 6000–8000 cm^{-1} in the calculated CT transition energies gives consistently good agreement with observation for a wide family of $4d^5$ and $5d^5$ hexahalometalates,[28] as directly confirmed here[29] for $[RuBr_6]^{3-}$ and $[OsBr_6]^{3-}$.

Taking a median value of 7000 cm^{-1} as the required empirical correction (*cf.* Table 4), the intense double bands centered around 32 000 cm^{-1} in $[Ru_2Br_9]^{3-}$ and 39 000 cm^{-1} in $[Os_2Br_9]^{3-}$ are readily assigned on energetic grounds to a combination of the $4a_2'' \rightarrow 7e''$ and $6e' \rightarrow 7e''$ transitions, augmented by $5e'' \rightarrow 9e'$, a conclusion reinforced by their exceptional computed oscillator strengths. Interestingly, charge transfer from $4a_2''$ is thoroughly mixed in character ($\sim^1/_3Br_{br}:^2/_3Br_t$) while the two higher components derive their intensity exclusively from terminal halide participation. These intense transitions are related to the $3t_{1u} \rightarrow 3e_g$ process[29] in the corresponding hexabromometalate. However, the same calculations effectively exclude an apparently obvious assignment of the structured near-UV/visible $[M_2Br_9]^{3-}$ envelope in terms of XMCT transitions into the lower-lying (t_{2g}-derived) $5a_2''$ orbital. Only the $5e'' \rightarrow 5a_2''$ CT transition falls in the appropriate energy range (after application of the 7000-cm^{-1} correction), and the calculated oscillator strength is much too low to account adequately for the observed spectrum.

Table 4. Calculated Transition Energies[a] (E) and Oscillator Strengths (f) for $[Os_2Br_9]^{3-}$ and $[Ru_2Br_9]^{3-}$

	$Ru_2Br_9^{3-}$		$Os_2Br_9^{3-}$	
transition	E/cm^{-1}	f	E/cm^{-1}	f
$6e'' \rightarrow 5a_2''$	5 300	0.057	7 200	0.071
$6a_1' \rightarrow 5a_2''$	**9 400**	**0.252**	**14 900**	**0.318**
$6e'' \rightarrow 7e''$	15 800	0.000	16 100	0.000
$8e' \rightarrow 7e''$	15 700	0.004	17 600	0.001
$6e'' \rightarrow 9e'$	20 500	0.004	21 300	0.001
$8e' \rightarrow 9e'$	20 400	0.000	22 800	0.000
$6a_1' \rightarrow 9e'$	**24 100**	**0.022**	**28 600**	**0.034**
$5e'' \rightarrow 5a_2''$	13 800	0.004	19 900	0.004
$4e'' \rightarrow 5a_2''$	19 600	0.037	27 400	0.057
$5e'' \rightarrow 7e''$	22 800	0.014	27 400	0.016
$7e' \rightarrow 7e''$	23 800	0.000	28 400	0.001
$5a_1' \rightarrow 5a_2''$	24 600	0.039	31 100	0.045
$1a_1'' \rightarrow 7e''$	24 200	0.000	28 900	0.000
$4a_2'' \rightarrow 7e''$	**24 100**	**0.138**	**29 100**	**0.154**
$4a_1' \rightarrow 5a_2''$	26 200	0.004	33 200	0.013
$6e' \rightarrow 7e''$	**26 700**	**0.090**	**31 700**	**0.108**
$2a_2' \rightarrow 9e'$	27 300	0.002	32 400	0.003
$5e'' \rightarrow 9e'$	**27 500**	**0.059**	**32 600**	**0.056**
$7e' \rightarrow 9e'$	28 500	0.000	33 600	0.000
$3e'' \rightarrow 5a_2''$	28 300	0.001	35 600	0.005
$4e'' \rightarrow 7e''$	30 500	0.046	35 100	0.056
$6e' \rightarrow 9e'$	31 400	0.062	36 800	0.072
$5e' \rightarrow 7e''$	32 700	0.283	38 300	0.324
$2e'' \rightarrow 5a_2''$	36 200	0.053	42 600	0.056
$4e'' \rightarrow 9e'$	35 200	0.071	40 300	0.073
$3a_2'' \rightarrow 7e''$	37 800	0.107	42 400	0.148
$1a_2' \rightarrow 9e'$	36 900	0.000	43 100	0.001
$5e' \rightarrow 9e'$	37 500	0.094	43 500	0.115
$3e'' \rightarrow 7e''$	36 700	0.117	43 400	0.110
$5a_1' \rightarrow 9e'$	38 800	0.231	44 300	0.341
$4a_1' \rightarrow 9e'$	40 200	0.088	46 200	0.020
$3e'' \rightarrow 9e'$	42 500	0.129	48 600	0.121

[a] A correction of 7000 cm^{-1} (see text) should be added to the energies of all the charge-transfer transitions; i.e. those below the break. Assignments advanced in the text are listed in **bold type.**

Linked to this problem is the absence in the visible/near-IR region of any intense absorption corresponding to the calculated $6a_1' \rightarrow 5a_2''$ ($\sigma \rightarrow \sigma^*$) transition; the first prominent feature lies some 8000–10 000 cm^{-1} higher in both complexes. In contrast, in the one-electron-reduced species,[25] $[Ru_2Br_9]^{4-}$, an intense band assigned to the $\sigma \rightarrow \sigma^*$ transition is observed at 10 200 cm^{-1}, close to the calculated energy. It is evident that while the promotion energy is calculated realistically for the $\sigma^2\sigma^{*1}$ configuration it is substantially underestimated for the even-electron $\sigma^2\sigma^{*0}$ systems. This is reminiscent of the behavior of the $\delta \rightarrow \delta^*$ transition in directly bonded M_2X_8 species, where the observed transition falls from 14 700 cm^{-1} for the even-electron ($\delta^2\delta^{*0}$) species, $[Re_2Cl_8]^{2-}$, to 7100 cm^{-1} for the reduced ($\delta^2\delta^{*1}$) species, $[Re_2Cl_8]^{3-}$.[30]

The effects of electron correlation on such transitions have been discussed by several authors.[31] Hopkins *et al.*[31b] developed a generally applicable expression for the observed transition energy, $h\nu$, where ΔW is the one-electron orbital separation (corresponding here to the Xα-calculated $\sigma \rightarrow \sigma^*$ transition energy in Table 4) and K is an electron-exchange term:

$$h\nu = K + (K^2 + (\Delta W)^2)^{1/2}$$

K is typically of the order of 8000 cm^{-1}, and taking this as a representative value, we would anticipate transitions near 20 000 cm^{-1} for $[Ru_2Br_9]^{3-}$ and near 25 000 cm^{-1} for $[Os_2Br_9]^{3-}$. The most prominent feature in the visible/near-UV envelopes are

(27) (a) Case, D. A.; Aizmann, A. *Inorg. Chem.* **1981**, *20*, 528. (b) Desjardins, S. R.; Penfield, K. W.; Cohen, S. L.; Musselman, R. L.; Solomon, E. I. *J. Am. Chem. Soc.* **1983**, *105*, 4590.

(28) McGrady, J. E.; Heath, G. A. *J. Chem. Soc., Dalton Trans.*, in press.

(29) The measured band maxima (*vs* calculated transition energies) are as follows: For $[RuBr_6]^{3-}$, $3t_{1u} \rightarrow 2t_{2g}$ = 22 500 (*vs* 14 500), $3t_{1u} \rightarrow 3e_g$ = 36 000 (*vs* 30 600) cm^{-1}; for $[OsBr_6]^{3-}$, $3t_{1u} \rightarrow 2t_{2g}$ = 28 000 (*vs* 19 400), $3t_{1u} \rightarrow 3e_g$ = 44 000 (*vs* 37 400) cm^{-1}.

(30) Heath, G. A.; Raptis, R. G. *J. Am. Chem. Soc.* **1993**, *115*, 3768.

(31) (a) Hall, M. B. *Polyhedron* **1987**, *6*, 679. (b) Hopkins, M. D.; Gray, H. B.; Miskowski, V. M. *Polyhedron* **1987**, *6*, 705. (c) Cotton, F. A.; Walton, R. A. *Multiple Bonds between Metal Atoms*, 2nd ed.; Oxford University Press: Oxford, United Kingdom, 1993; p 682.

indeed found at 19 800 and 24 300 cm^{-1}, respectively; these bands are then logically assigned to the $\sigma \rightarrow \sigma^*$ transition, resulting in revised K values of 7700 cm^{-1} in both cases. The corresponding bands in $[RuCl_9]^{3-}$ and $[Os_2Cl_9]^{3-}$ are found at 22 600 and 28 700 cm^{-1}. Thus, contrary to previous reports,[20,25] the intense $\sigma \rightarrow \sigma^*$ absorption of $Ru_2X_9^{3-}$ should neither be dismissed nor located below 13 000 cm^{-1}.

The remaining excitation anticipated in the visible near-UV region (cf. Table 4) is $6a_1' \rightarrow 9e'$, which is formally related to the single-ion ligand-field promotion. Generally such transitions are rather accurately located by $X\alpha$ methods. Although these processes are forbidden in octahedral symmetry, they gain intensity in the bimetallic species due to the absence of an inversion center. Accordingly, we believe that $6a_1' \rightarrow 9e'$ is more likely to contribute to the observed envelope than the $5e'' \rightarrow 5a_2''$ charge-transfer transition discussed above, where the calculated oscillator strength is at least five times smaller.

Conclusions

In summary, the X-ray determination of $Rb_3O_8Br_9$ has enabled explicit theoretical comparison of bonding interactions in the 4d and 5d 10-e confacial nonabromide systems. The optical spectra and the magnetochemical data (5–300 K)[1,2] are readily interpreted in this context. The preliminary attribution[20] of a strong direct M–M bond in $[Ru_2X_9]^{3-}$ is more appropriate to $[Os_2X_9]^{3-}$. Such 4d *vs* 5d comparisons within the nonahalides were previously available only for the multiple bonded Mo and W systems, where changes in the strength of both σ and δ_π bonding occur. Thus, the comparison between the tervalent Ru and Os systems provides a unique opportunity to study the σ bond in isolation. Heath and Kennedy[32] have recorded the solution spectra of electrogenerated 10-e $[Ir_2Cl_9]^-$ and $[Ir_2Br_9]^-$, but it is not likely that these highly reactive species or their transient Rh(IV) counterparts can be crystallographically characterized.

Acknowledgment. We thank Siegbert Schmidt and John Thompson (RSC) for generous assistance with preliminary powder-diffraction measurements. This work was supported financially by the ANU Institute of Advanced Studies, by an Australian CPRA award to D.G.H, and by a SERC (U.K.) overseas studentship to J.E.M.

Supplementary Material Available: Tables listing anisotropic displacement parameters, interatomic distances, interatomic angles, torsion angles, nonbonded contacts, and molecular orbital energies and compositions for $[RuBr_6]^{3-}$, $[Ru_2Br_9]^{3-}$, $[OsBr_6]^{3-}$, and $[Os_2Br_9]^{3-}$ (6 pages). Ordering information is given on any current masthead page.

(32) Heath, G. A.; Kennedy, B. J. Manuscript in preparation.